Available online at www.sciencedirect.com
ScienceDirect
Journal of the European Ceramic Society 30 (2010) 17–28
www.elsevier.com/locate/jeurceramsoc

Porous single-fired wall tile bodies: Influence of quartz particle size on tile properties

J.L. Amorós *, M.J. Orts, S. Mestre, J. Garcia-Ten, C. Feliu

Instituto de Tecnología Cerámica, Asociación de Investigación de las Industrias Cerámicas, Universitat Jaume I, Castellón, Spain

Received 12 March 2009; received in revised form 26 June 2009; accepted 3 August 2009
Available online 31 August 2009

Abstract

This study examines the effect of quartz particle size in raw material composition customarily used for the manufacture of porous single-fired wall tile bodies on the characteristics of the green tiles and on the thermal and mechanical properties of the fired tiles. Quartz particle size was varied, while the quantity and particle size of the other raw materials were kept constant. Tile compacts were formed by uniaxial pressing and fired at different peak temperatures. The resulting fired microstructure was then characterised and tile thermal and mechanical properties were determined. Microcrack formation around quartz particles leads to hysteresis of the coefficient of thermal expansion during heating and cooling. The studied mechanical and thermal properties are shown to be a function of the magnitude of the hysteresis and porosity. This relationship is independent of the operating variables (pressing pressure, operating temperature, and quartz particle size) used. The results obtained confirm that the green and fired properties of porous single-fired wall tiles may be considerably enhanced, while holding low shrinkage and high porosity, compatible with low moisture expansion, by reducing quartz particle size and appropriately adjusting the pressing pressure and peak firing temperature. This should enable thin and/or large-sized porous wall tiles to be manufactured, without (immediate or delayed) curvatures, and with a higher breaking load than that required by the standards.

Keywords: Thermal expansion; Mechanical properties; Porosity; Final microstructure; Traditional ceramics

1. Introduction

Annual wall tile production currently stands at more than $4 \times 10^8\,m^2$ in Europe, with turnover exceeding 3×10^9 €/annum. The greatest demand in wall tiles in recent years has been for thin, large-sized, white-firing earthenware tiles. For the manufacture, by single firing, of these thin glazed sheets with high porosity (water absorption ≥15%), without immediate or delayed curvatures, and with an appropriate breaking load, it is essential, among other factors, that the tiles should have good (green and fired) mechanical properties.

The raw materials mixture contains a balanced proportion of plastic materials (clays) and non-plastic materials (calcium carbonate, quartz, or feldspathic sands), which are milled to a particle size that allows green tiles to be pressed with appropriate green mechanical strength, whose constituents will react in the short firing cycles used in industrial practice[1–4] (≈40 min). Calcium carbonate needs to have a small particle size in order to decompose rapidly and completely during the first stages of the firing cycle, while the resulting calcium oxide must fully react with clay minerals decomposition products to produce calcium aluminosilicates and/or calcium magnesium aluminosilicates[5–7] (if calcium magnesium carbonate is used). Pinholes would otherwise develop in the glazed surface and/or the end product would contain amorphous phases, or even residual calcium oxide, which could hydrate, damaging the tiles[8–11] (leading to delayed curvatures, crazing, etc.). Quartz is a cheap lightweight raw material, a relatively large quantity of which (35–50 wt%) is needed in the body composition, partly as siliceous clays (quartz content of 15–30 wt%) and partly as feldspathic sands (quartz content above 60 wt%), mainly for two reasons. First, because quartz is the principal determining component of the high mean coefficient of thermal expansion of the resulting tile, which is required in order to obtain an appropriate glaze-body fit. Secondly, because quartz acts as a filler and contributes to dimensional stability by reducing firing shrinkage.

The effect of quartz[12] (grain size and content) on the mechanical properties of porous wall tile has received little attention,

* Corresponding author.
E-mail address: jlamoros@itc.uji.es (J.L. Amorós).

0955-2219/$ – see front matter © 2009 Elsevier Ltd. All rights reserved.
doi:10.1016/j.jeurceramsoc.2009.08.001

especially in regard to particle size. This is in sharp contrast with the abundant information available on porcelain, vitreous china sanitary ware, and porcelain tile. For these materials, with abundant glassy phase and low porosity, the principal factor influencing strength is considered to be quartz particle size, as demonstrated repeatedly by several researchers.[13–18] This effect is basically caused by two simultaneously acting mechanisms related to the difference between the coefficients of thermal expansion of the quartz and of the glassy matrix: on the one hand, the difference in thermal expansion between both materials has a strengthening effect, by subjecting the glassy matrix to microscopic residual compressive stress; on the other, the magnitude of the stresses produces cracks around the quartz particles when quartz particle size exceeds a critical size, a_c, thereby causing partial stress relaxation and increasing microstructural damage, which may even lead to particle detachment. This microstructural damage adversely affects the product's mechanical properties.

In porous wall tile bodies, whose microstructure and composition differ entirely from those of porcelain bodies (higher porosity and smaller glassy phase content), the foregoing two mechanisms also need to be considered, albeit in a different measure. Thus, the presence of cracks around and within the large quartz particles has also been observed.[12]

One way of estimating the extent to which microcracking develops during tile cooling in the kiln is by determining the hysteresis of the coefficient of thermal expansion around 573 °C during heating and cooling of a fired test piece in a dilatometer.[19,20] The magnitude of the hysteresis of the thermal expansion has been shown to determine the thermal and mechanical properties in anisotropic and/or composite materials.[21–24] This hysteresis effect between heating and cooling, observed for these sintered materials, has also been attributed to the occurrence and recombination of microcracks.

This study examines the effect of quartz particle size in raw material composition customarily used for the manufacture of porous single-fired wall tile bodies on the characteristics of the green tiles and on the thermal and mechanical properties of the fired tiles. Quartz particle size was varied, while the quantity and particle size of the other raw materials were kept constant. Tile compacts were formed by uniaxial pressing and fired at different peak temperatures. The resulting fired microstructure was then characterised and tile thermal and mechanical properties were determined.

This study has two objectives. The first is to determine the effect of quartz particle size on the mechanical and thermal properties of the fired body, and to attempt to relate these properties to the fired tile's main characteristics (porosity, phase content, microstructure, etc.). Indeed, determining how microcrack density, estimated by thermal expansion hysteresis, affects the above properties constitutes an important new approach. The second objective is to explore the possibility of improving fired tile mechanical strength, reducing quartz particle size and appropriately modifying the operating variables, while holding or improving the other key characteristics and properties of the semi-processed and the finished product. The purpose of the foregoing is to enable thin and/or large-sized porous wall tiles to be made, without (immediate or delayed) curvatures, with a higher breaking load than that required by the standards.

Table 1
Raw materials chemical composition.

wt%	E-clay	S-clay	Quartz	Calcite	K-feldspar
SiO_2	63.2	64.0	98.7	0.2	68.7
TiO_2	1.3	1.01	0.08	–	0.03
Al_2O_3	23.8	20.2	0.54	0.1	17.3
Fe_2O_3	1.2	2.35	0.05	0.05	0.14
MgO	0.4	0.36	0.01	0.2	0.05
CaO	0.3	0.55	0.01	55.7	0.44
Na_2O	0.3	0.17	0.04	–	2.20
K_2O	2.6	2.09	0.32	0.01	10.61
l.o.i.	6.8	6.60	0.25	43.5	0.52

2. Materials and procedure

The following raw materials were used: an English ball clay, E-clay (HSM clay from Imerys Tiles Minerals), a white clay from Teruel (Spain), S-clay (Roma clay from Minera Sabater, containing mainly kaolinite, micaceous material, and free quartz); calcite (from Zaera, Calaf); potassium feldspar (FK-100 from Incusa, also containing sodium feldspar); and three quartz sands from Sibelco of the same composition (containing traces of potassium feldspar), but having a different particle size distribution (PSD): F-quartz, M-quartz, and C-quartz, for fine, medium and coarse quartz particle sizes, respectively. Apart from the English ball clay, the raw materials were from Spain and are widely used in manufacturing white-body earthenware tiles.

The chemical composition of the raw materials is given in Table 1. The corresponding particle size distributions are detailed in Table 2.

Three different slips were prepared consisting of 45% S-clay, 10% E-clay, 15% calcite, 5% K-feldspar, and 25% quartz of different grain size.

Slurries were prepared by dispersion with a high-speed disperser. Slurry loading was 65 wt%, deflocculant content being 0.5 wt% of a sodium metasilicate–sodium tripolyphosphate mixture in a 3:1 ratio. Stirring time was 1 h. Slurry viscosity was measured as a function of shear rate between 10^{-1} and 10^{3} s^{-1}.[25]

The suspensions were spray dried at 200 °C in a laboratory spray dryer. Prior to compaction, the moisture content of the

Table 2
Cumulative particle size distribution.

	Particle size (μm)				
	<10%	<25%	<50%	<75%	<100%
E-clay	–	–	0.5	3.5	21
S-clay	–	–	1.1	6.0	20
Calcite	2.4	4.7	9.1	17.4	28.5
K-feldspar	1.5	3.5	10.9	23.0	35.5
C-quartz	3.9	35.3	41.8	83.4	129
M-quartz	2.5	8.3	23.0	44.3	67.3
F-quartz	2.4	4.6	7.9	14.1	23.1

three spray-dried powders was adjusted to 0.05 kg water/kg dry solid. The powders obtained were stored for at least 72 h.

Disk-shaped test specimens, 45 mm in diameter and 5 mm thick, were prepared by compacting the three spray-dried powders in a cylindrical steel die at a rate of 1 mm/min up to different maximum pressures: 17, 22, and 40 MPa.

Since compactness, ϕ, of the green tile significantly influences tile properties and characteristics in both the green and fired state, and the modification of quartz particle size alters compactness, in order to isolate the effect of particle size on compactness, two series of test pieces were formed. In one series, pressing pressure was held at the value customarily used for these products ($P = 22$ MPa). In the other series, pressing pressure was judiciously modified to obtain a constant green compactness of $\phi = 0.74$.

In order to carry out mechanical testing, bars were formed by pressing each powder at different maximum pressures. The resulting compacts were dried at 110 °C for 3 h. The dried bars and disks were fired in an electric laboratory kiln at three different peak temperatures: 1050, 1100, and 1150 °C. The heating rate was 2400 °C/h, with a 6-min hold at peak temperature. The firing cycle was similar to that commonly used in single-fired earthenware tile manufacture.

Test compact porous texture was characterised by measuring bulk density and water absorption. Pore size distribution (PSD) was determined by mercury porosimetry.

Linear thermal expansion of the fired bodies was measured in a high temperature thermal dilatometer by heating up to 900 °C and subsequent cooling at a rate of 5 °C/min.

In order to determine green and fired mechanical strength and Young's modulus of the fired pieces, three-point bend tests were performed on the 80 mm × 20 mm × 7 mm bars. The distance between the two roller supports was 60 mm. Crosshead speed during all mechanical testing was 1 mm/min.

SEM studies and EDS analysis were performed on polished and etched samples (3 s in 5 wt% HF) and on fracture surfaces. Polished specimens were observed in the backscattered mode. Quantitative XRD studies by Rietveld analysis were conducted to follow phase development on firing.

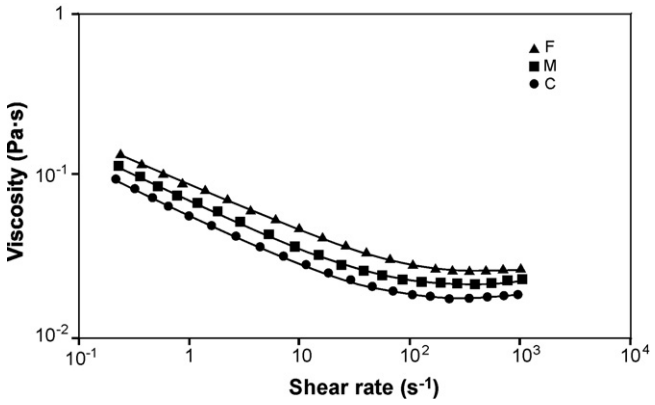

Fig. 1. Flow curves of the suspensions prepared with fine (F), medium (M), and coarse (C) quartz particles.

3. Results and discussion

3.1. Slurry rheology

Fig. 1 shows the flow curves of the suspensions prepared with C-quartz, M-quartz, and F-quartz. They exhibit shear thinning at low and moderate shear rates, followed by a dilatant segment.

As reported elsewhere,[25] this rheological behaviour is typical of well-deflocculated, highly concentrated clay suspensions. Under shear conditions in which the suspensions exhibit shear thinning, this behaviour is found to fit the Sisko equation:

$$\eta = \eta_\infty + k\dot{\gamma}^{-1} \quad (1)$$

In all three cases, the variation of viscosity (η) with shear rate (γ) around the flow curve minimum (η_∞) is very small or practically zero, so that suspension behaviour can be considered virtually Newtonian in this high shear range where hydrodynamic forces are very high and dominant. The decrease in viscosity as quartz particle size increases may be caused by an increase in maximum packing fraction of the suspension.

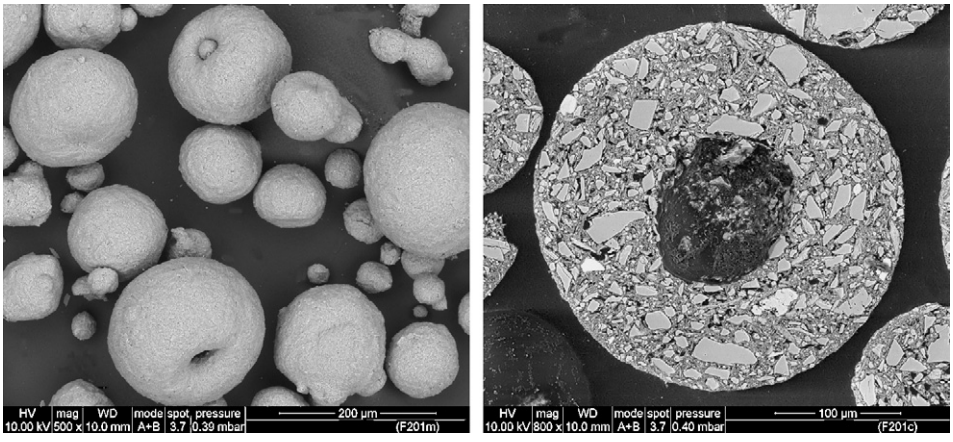

Fig. 2. Surface and cross-section of spray-dried granules.

Table 3
Compaction behaviour. Parameters 'm' and 'n' of Eq. (2).

Type of quartz	m	n
Coarse	0.5859	0.0531
Medium	0.5744	0.0533
Fine	0.5477	0.0526

3.2. Granule characteristics and their compaction behaviour

Fig. 2 shows typical granules used in this study. The granules were hollow, roughly spherical, and contained a single large spherical cavity connected to the external surface by a single large channel, like the granules obtained in industrial spray dryers.[26] No significant differences were found between the characteristics of the granules obtained with each of the three test quartzes.

The relative density or compactness of the green disks, ϕ, increased in proportion to the logarithm of compaction pressure (P) according to the following equation:

$$\phi = m + n \ln P \quad (2)$$

Table 3 presents parameters 'm' and 'n' of Eq. (2). The 'm' values are similar for the three spray-dried powders, indicating that the effect of pressure on compaction, at least in the range of pressures used, is independent of quartz particle size distribution. In contrast, parameter 'n' rises as quartz particle size increases, just as disk compactness does under the same compaction pressure, because a larger average quartz particle size and a broader quartz particle size distribution improve particle packing density.[27]

3.3. Green compact pore size distribution and mechanical strength

Fig. 3a and b shows that the pore size distribution of disks made from the spray-dried powders containing C, M, and F-quartz is monomodal, intergranular pores not being detected. However, there are some differences between the C, M, and F curves, especially in the larger-pore range.

Table 4
Compactness, ϕ, and mechanical strength, σ_d, of green test bars made from C-quartz, M-quartz, and F-quartz.

Type of quartz	Test bars	P (MPa)	ϕ	σ_d (MPa)
Coarse	C22	22	0.7475 ± 0.0008	3.03 ± 0.11
Medium	M22	22	0.7400 ± 0.0005	2.91 ± 0.07
Fine	F22	22	0.7075 ± 0.0005	2.50 ± 0.07
Coarse	C17	17	0.7393 ± 0.0005	2.86 ± 0.07
Fine	F40	40	0.7410 ± 0.0007	3.54 ± 0.11

It may be inferred from Fig. 3b (green PSD of $\phi = 0.74$) that at the same compaction, the pores in the resulting compacts become larger when the composition coarse quartz particle fraction (quartz particle size) increases. These findings are in agreement with the literature,[27] and confirm that particle size is directly related to pore size in the green packing. The same trend is also observed, albeit less noticeably, in the curves corresponding to pressures of 22 MPa.

Table 4 details the green mechanical strength, σ_d, of the test bars made under standard pressing conditions ($P = 22$ MPa), and of the series prepared at different pressures to attain the same compaction ($\phi = 0.74$), with spray-dried powder containing C, M, and F-quartz. Twelve bars were tested for each operating condition. The compactness values, ϕ, of the test bars are also given.

When the results of test pieces C17, M22, and F40, which have about the same compactness ($\phi = 0.74$), are compared, the pieces made with fine quartz (F40) are observed to display considerably greater strength than those prepared with the other quartzes. This is consistent with the simplest theoretical models, which predict that, at the same compactness, ϕ, compact mechanical strength increases as particle size decreases. This effect is negligible when the results corresponding to the bars pressed using medium (M22) and coarse (C17) quartz sizes are compared. However, the results corresponding to the bars formed at the usual pressing pressure, $P = 22$ MPa (F22, M22, and C22), display a clear relationship between test piece compactness and mechanical strength, confirming the notable influence of this characteristic on the mechanical performance of the green compact, extensively described in the literature.[28–30]

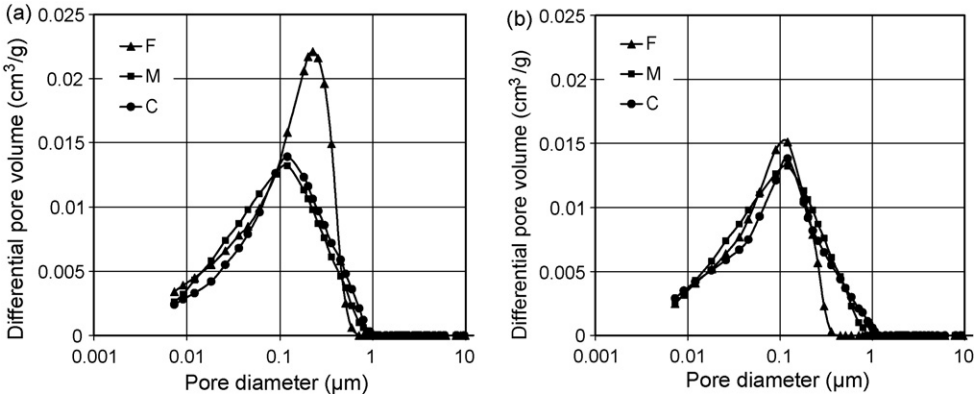

Fig. 3. Pore size distribution of green compacts. $P = 22$ MPa series (3a) and $\phi = 0.74$ series (3b).

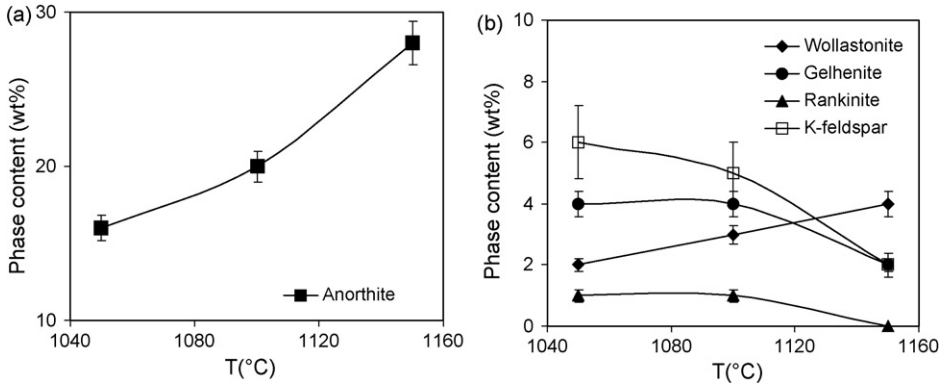

Fig. 4. Variation of crystal phase content with temperature. Anorthite (4a) and minor phases (4b).

3.4. Fired compact properties

3.4.1. Phase analysis

The X-ray diffraction patterns showed that neoformed calcium-based phases (gehlenite/melilite, anorthite/plagioclase, and wollastonite) occurred in all fired test compacts and that the corresponding phase contents were independent of quartz particle size distribution and the compaction variables used. Fig. 4 shows how crystalline phase content, except quartz, evolves with firing temperature. As firing temperature rises, the anorthite/plagioclase (the major phase) content increases (Fig. 4a), while the gehlenite content decreases (Fig. 4b). These results match those reported for fired calcareous clays[2,6,31,32] and suggest that gehlenite, produced by reaction between clay mineral decomposition products and CaO, decreases by reaction with amorphous clay products (and also probably with the finest quartz particles), forming anorthite/plagioclase. As firing temperature rises, the wollastonite content increases (Fig. 4b) due to the reaction between gehlenite and fine quartz grains or by reaction of the remaining CaO and fine quartz grains. On the other hand, as firing temperature rises, K-feldspar (Fig. 4b) and quartz content (Fig. 5) decrease.

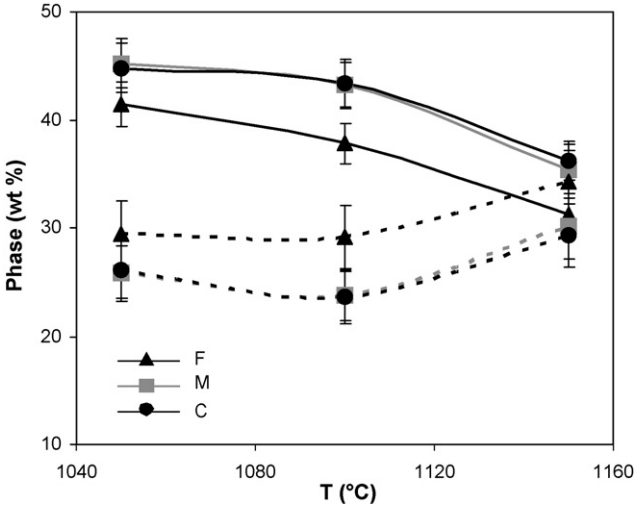

Fig. 5. Evolution of quartz (solid line) and amorphous phase (dashed line) content with temperature, for test pieces with fine (F), medium (M), and coarse (C) quartz particles.

At the three test firing temperatures, the pieces prepared with the finest quartz (F-quartz) contained less quartz than the other pieces (with M-quartz and C-quartz). In addition, the quartz content of the pieces with M-quartz and C-quartz was similar. Fig. 5 shows the variation of the amorphous phase content with firing temperature for the test pieces. The pieces fired at 1050 and 1100 °C are observed to have practically the same amorphous phase content, which increases in the pieces fired at 1150 °C.

3.4.2. Microstructure analysis

The polished surfaces of the pieces fired at 1050 °C exhibit a large amount of porosity (represented by black areas) with a broad range of pore sizes (Fig. 6). The irregular shape of the pores and presence of quartz grains with sharp edges are characteristic of a low degree of liquid-phase sintering. In addition, large pores from calcite decomposition with bright edge rims due to high calcium content are also evident.[33]

The pieces fired at 1100 °C have a similar microstructure to those fired at 1050 °C. However, the pieces fired at 1150 °C display more extensive vitrification with increased liquid-phase content (Fig. 7). The liquid-phase suppresses the small pores and facilitates quartz dissolution, rounding quartz particle edges and reducing the number of small pores. Residual pores also become rounded. More dense zones are observed as a result of

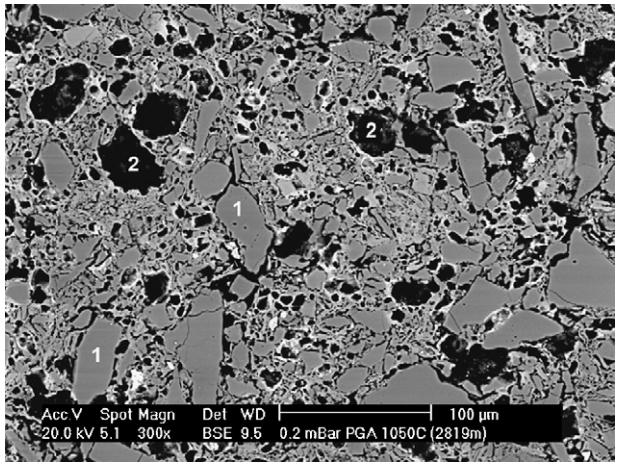

Fig. 6. Polished cross-section of a test piece fired at 1050 °C. Quartz particle: 1. Pore: 2.

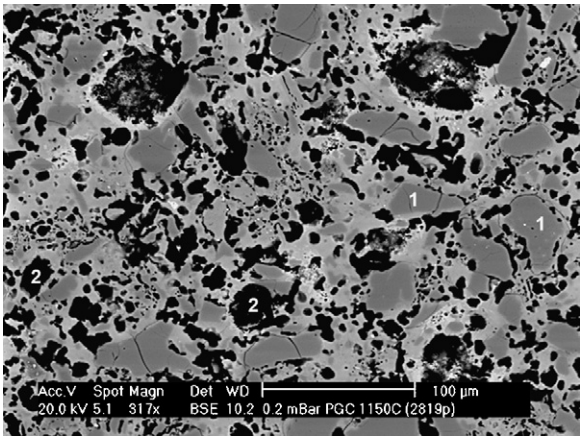

Fig. 7. Polished cross-section of a test piece fired at 1150 °C. Quartz particle: 1. Pore: 2.

the liquid phase, which becomes a glassy matrix on cooling. Moreover, in all pieces, the presence of microcracking around and within large quartz grains is clearly visible. These cracks, acting by themselves or in combination with large pores, constitute fracture-initiating flaws that contribute to body failure. Such microcracking results from the thermal expansion mismatch on cooling between quartz grains and the surrounding matrix, mainly around 573 °C. However, some cracked grains may also have been generated as a result of the stress induced during polishing, as quartz grains were already stressed when cooled.

The etched polished surfaces of the test pieces fired at 1050 °C exhibit very small spheroid crystals, which are brighter than the rest of the piece, forming clusters on the pore boundaries (Fig. 8). Energy-dispersive spectroscopy (EDS) analysis (Fig. 9) shows that these crystals are mainly made up of calcium, aluminium, silicon, and oxygen while they also contain small quantities of potassium and iron. They could therefore be gehlenite crystals or a mixture of gehlenite and rankinite crystals. A large quantity

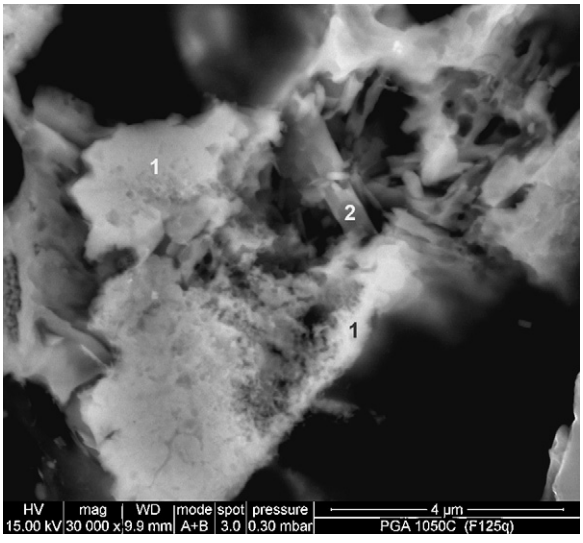

Fig. 8. Etched polished cross-section of a test piece fired at 1050 °C. Spheroid crystals: 1. Needle-like crystals: 2.

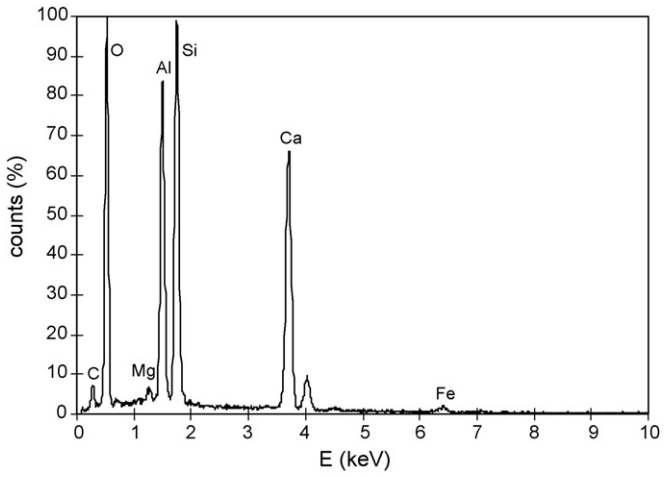

Fig. 9. EDS analysis of spheroid crystals in Fig. 8.

of elongated, needle-like crystals (Fig. 8) may be observed, randomly oriented near large pores, embedded in the glassy matrix. The EDS findings (Fig. 10) are consistent with an anorthite composition for those crystals.[2]

The anorthite and gehlenite crystals were found to have grown considerably in size and quantity in the pieces fired at 1150 °C (Fig. 11). These findings match the XRD data, which show a higher anorthite and gehlenite crystal content. However, crystal chemical composition is quite similar in the pieces fired at 1050 and 1150 °C.

The detection of small quantities of iron in the anorthite and gehlenite crystals confirms that both phases can accommodate some ferric iron, replacing the aluminium sites, and preventing or reducing haematite crystallisation, which thus explains the whitening effect of calcareous compositions.

3.4.3. *Porosity and pore size distribution*

The pore size distributions of the M22 series, comprising test pieces fired at different temperatures, are plotted in Fig. 12. Their apparent porosity (ε_A) and true porosity (ε) are given in Table 5. Although a rise in firing temperature hardly modifies porosity, the results confirm that the intrusion curves progressively shift

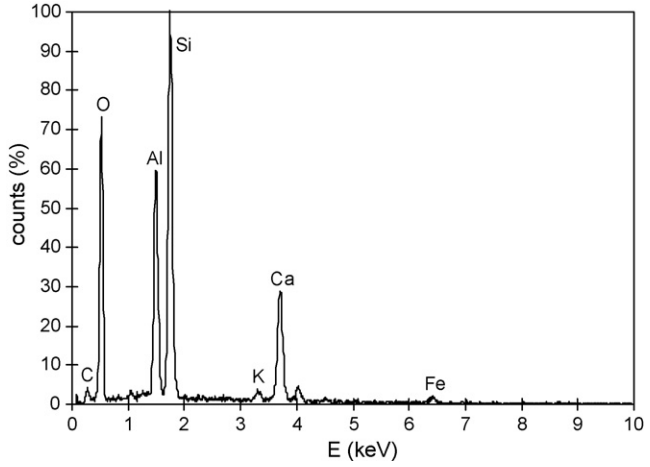

Fig. 10. EDS analysis of needle-like crystals in Fig. 8.

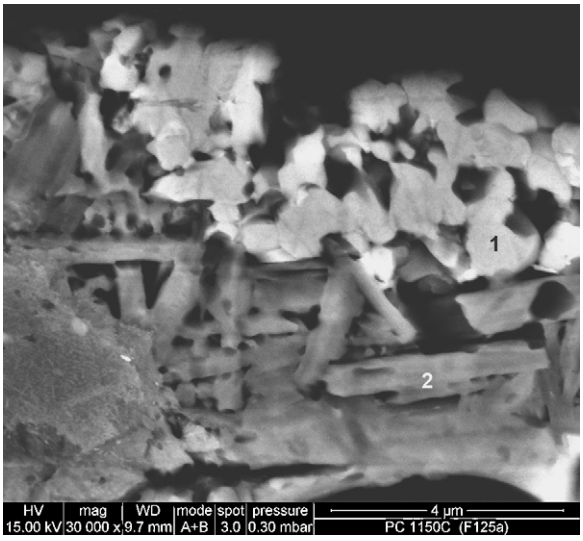

Fig. 11. Etched polished cross-section of a test piece fired at 1150 °C. Spheroid crystals: 1. Needle-like crystals: 2.

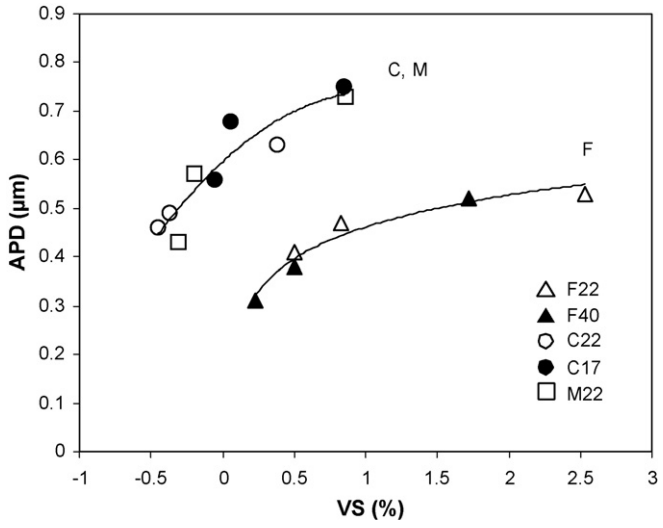

Fig. 13. Variation of average pore diameter (APD) with volumetric shrinkage (VS).

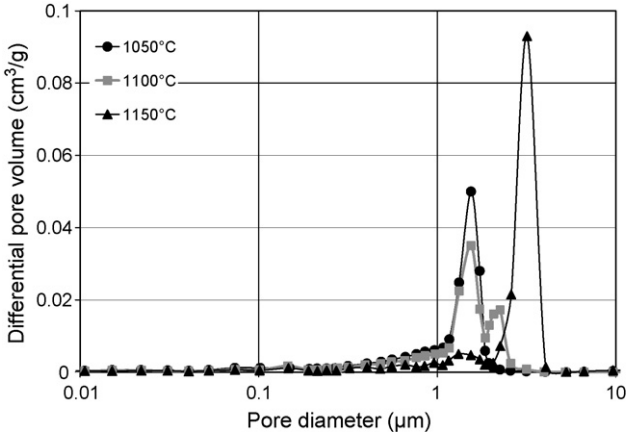

Fig. 12. Pore size distribution of M22 test pieces fired at different temperatures.

towards larger-pore sizes (Fig. 12). Such coarsening during sintering (Table 5) is the result of heterogeneous pore sizes in the green packing (Fig. 3).

In order to analyse the relationship between pore growth and degree of sintering, the average pore diameter (APD) has been plotted versus volume shrinkage (VS) in Fig. 13. When densification increases, APD grows.[34] Greater initial particle packing heterogeneity, i.e. when the green body contains larger quartz particles (the case of the C and M pieces), raises the APD growth rate (curve slope). Pore growth with temperature in initial- and intermediate-stage sintering in the presence of liquid phase has been observed in clay compositions and in glassy materials.[27,35] This is due to elimination of the smaller pores, leading to differential shrinkage of the material and larger-pore growth.

The evolution with temperature of pore size distribution, at constant pressure or compaction, is alike for all series, the only difference being that for some series the curves are just bimodal for the test pieces fired at 1150 °C. Raising the temperature causes the coarsest pores to grow. When the green

Table 5
Characteristics of the fired test pieces.

Test piece	P (MPa)	T (°C)	VS (%)	WA (%)	ε_A	ε
C22-1	22	1050	−0.45 ± 0.06	16.9 ± 0.7	0.302 ± 0.009	0.3260 ± 0.0006
C22-2	22	1100	−0.37 ± 0.08	16.8 ± 0.8	0.299 ± 0.010	0.3279 ± 0.0006
C22-3	22	1150	+0.38 ± 0.09	16.6 ± 0.5	0.297 ± 0.006	0.3256 ± 0.0002
M22-1	22	1050	−0.31 ± 0.05	17.5 ± 0.8	0.309 ± 0.010	0.3332 ± 0.0006
M22-2	22	1100	−0.20 ± 0.05	17.8 ± 0.6	0.314 ± 0.007	0.3343 ± 0.0003
M22-3	22	1150	+0.86 ± 0.02	16.9 ± 0.8	0.300 ± 0.010	0.3309 ± 0.0008
F22-1	22	1050	+0.50 ± 0.03	19.8 ± 0.7	0.337 ± 0.008	0.3584 ± 0.0006
F22-2	22	1100	+0.83 ± 0.03	19.9 ± 0.6	0.338 ± 0.007	0.3592 ± 0.0005
F22-3	22	1150	+2.53 ± 0.05	18.5 ± 0.4	0.318 ± 0.005	0.3524 ± 0.0004
C17-1	17	1050	−0.06 ± 0.03	17.6 ± 0.3	0.309 ± 0.005	0.3385 ± 0.0004
C17-2	17	1100	+0.06 ± 0.02	18.5 ± 0.6	0.324 ± 0.007	0.3400 ± 0.0003
C17-3	17	1150	+0.85 ± 0.05	17.9 ± 0.6	0.314 ± 0.008	0.3374 ± 0.0005
F40-1	40	1050	+0.23 ± 0.02	16.0 ± 0.9	0.284 ± 0.010	0.3294 ± 0.0006
F40-2	40	1100	+0.50 ± 0.05	15.6 ± 0.5	0.277 ± 0.006	0.3294 ± 0.0002
F40-3	40	1150	+1.72 ± 0.05	15.3 ± 0.4	0.275 ± 0.005	0.3230 ± 0.0004

VS: volumetric shrinkage (−expansion, +shrinkage). WA: water absorption. ε_A: apparent porosity. ε: porosity.

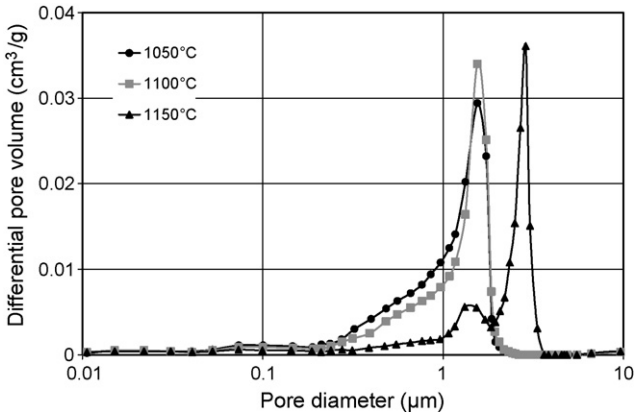

Fig. 14. Pore size distribution of C17 test pieces fired at different temperatures.

body contains larger pores (the case of the C17 series (Fig. 14)), the pore growth rate increases. These findings show that, during sintering, pore size growth depends on pore size in the green body, even in bodies with low liquid-phase formation.

3.4.4. Thermal expansion

It is well known that free quartz provides clay-based ceramic bodies with a high mean coefficient of linear thermal expansion, α. In this study, α is the mean coefficient of linear thermal expansion in the 100–650 °C range. Therefore, in each test series, an increase in firing temperature may generally be assumed to reduce α, mainly owing to the partial dissolution of quartz. When the results of the series that differ solely in their pressing conditions are compared, this variable displays no clear trend. However, when the α values corresponding to the test pieces with fine quartz particles are compared with those containing coarse quartz particles, it may be observed that though the pieces containing coarse quartz particles have a larger residual quartz content at the same firing temperature, their coefficient of thermal expansion is smaller (Fig. 15). This apparent contradiction can be explained by the microcracking phenomenon.

Microcracking can be correlated with the hysteresis of the coefficient of thermal expansion during heating and cooling

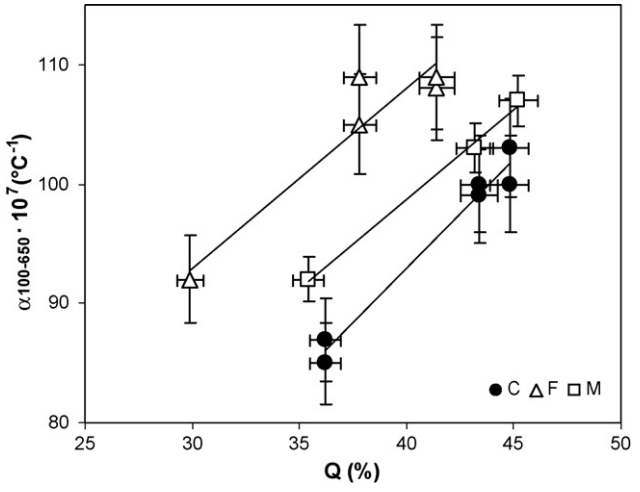

Fig. 15. Mean linear thermal expansion coefficient as a function of residual quartz content.

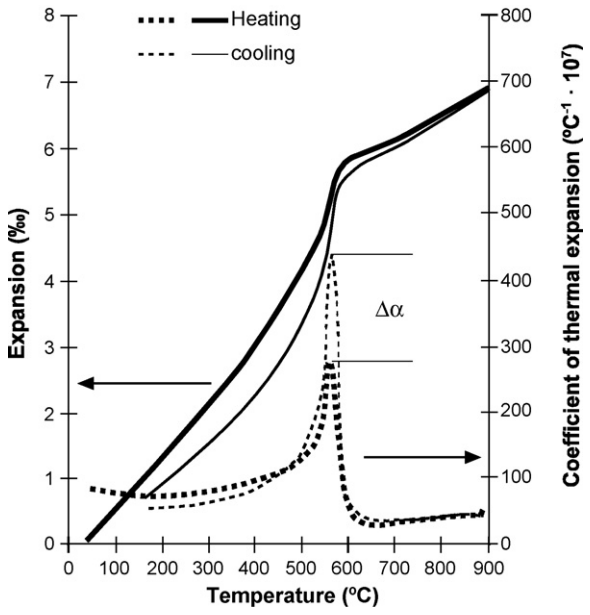

Fig. 16. Thermal expansion curve.

(Fig. 16). The origin of the hysteresis appears to be related to microcrack formation in the tile during cooling in the kiln, since the quartz coefficient of expansion is larger than that of the other existing phases (glassy phase, anorthite, gehlenite, etc.).[19,20] As a result, during heating of the fired piece in a dilatometer, only a fraction of the quartz present in the compact, Q, namely the quartz joined to the matrix, Q_j, contributes to overall expansion since many quartz particles are separated from the matrix (detached quartz, Q_d) by microcracks, which accommodate particle expansion. At dilatometer peak test temperature (900 °C), which is higher than the transformation temperature of the glassy phase in the matrix, the quartz particles are rebonded to the matrix.

During cooling in the dilatometer, the existing phases remain bonded until a temperature of about 573 °C is reached, because down to about this temperature the coefficients of thermal expansion of all phases are similar and the cooling rate is slow. When the quartz shrinks abruptly at 573 °C, almost all the quartz is joined to the matrix and contributes to overall tile shrinkage. As a result, at this temperature, the test piece coefficient of thermal expansion during cooling must be greater than that found during heating. In accordance with this assumption, the magnitude of the hysteresis (measured as $\Delta\alpha$, Fig. 16), must be directly related to microcrack concentration,[19,20] or to the quartz content detached from the matrix, Q_d. Thus, $Q_d \approx K\,\Delta\alpha$, where K is a proportionality constant.

In order to analyse the dependence of α on Q_j, it has been assumed that α increases linearly with the quartz content joined to the matrix, Q_j, during heating of the test piece in the dilatometer and that Q_j is the difference between total quartz content, Q, and detached quartz content, Q_d, thus yielding:

$$\alpha = a + bQ_j = a + b(Q - K\,\Delta\alpha) \tag{3}$$

where a, b, and K are fitting parameters.

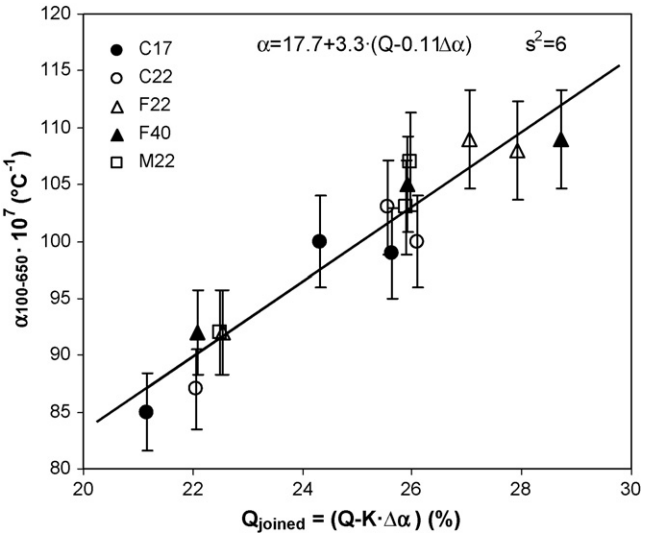

Fig. 17. Experimental α values versus calculated joined quartz content.

It has been attempted to fit the experimental values of α, $\Delta\alpha$, and Q to Eq. (3). Fig. 17 plots the experimental α data versus the calculated joined quartz content, Q_j. As can be seen, all data fit quite well a straight line of positive slope (variance, $s^2 = 6$), according to Eq. (3).

These outcomes show that α increases linearly with joined quartz content, Q_j, as had been assumed, and that this relationship is independent of the operating variables used. Thus, the introduction of a single structural parameter, Q_j, which can be readily estimated and has a simple physical meaning, enables the effect of the different operating variables on α, in materials as complex as those used in this study, to be explained.

3.5. Mechanical properties

The mechanical and thermal properties of the pieces fired at the three test temperatures are detailed in Table 6. Twelve bars were mechanically tested for each series. The table indicates the following:

(i) Each series generally shows an increase in mechanical strength, σ, and modulus of elasticity, E, with firing temperature, the effect of this variable being much more pronounced when the temperature rises from 1100 to 1150 °C. These effects can be related, in principle, to a series of mineralogical and microstructural transformations that develop parallel during firing, and whose degree of progress depends, therefore, on peak firing temperature, as indicated previously. Thus, anorthite formation and quartz dissolution, with the ensuing formation of glassy phase, are transformations whose greatest degree of development occurs between 1100 and 1150 °C, which could explain, in principle, why mechanical properties improve with firing temperature. In this sense it may be noted that sintering progress of the pieces in all test series is evidenced by average pore size growth, while total porosity remains practically steady, in accordance with what has been observed for these types of compositions.[6,7,31]

(ii) Comparison of the results corresponding to test pieces made using quartz of the same particle size, fired at the same temperature (C22–C17, F22–F40), generally shows that increased green compactness, caused by higher pressing pressure, leads to denser fired pieces with better mechanical properties.[20]

(iii) At the same firing temperature, both the data corresponding to the test pieces with constant ϕ (C17, M22, and F40) and the data corresponding to test pieces formed at $P = 22$ MPa (C22, M22, and F22) show that the Young modulus, E, and mechanical strength, σ, increase as average quartz particle size decreases. This trend may be due to a series of factors related to initial quartz particle size. Thus, a decrease in initial quartz particle size leads, generally, except for the results corresponding to the M and C test pieces at

Table 6
Mechanical and thermal properties of the fired test pieces.

Test piece	P (MPa)	T (°C)	σ (MPa)	E (GPa)	$\alpha_{100–650} \times 10^7$ (°C^{-1})	$\Delta\alpha \times 10^7$ (°C^{-1})
C22-1	22	1050	15.7 ± 0.7	8.2 ± 0.4	103 ± 3	170 ± 3
C22-2	22	1100	17.0 ± 0.8	8.1 ± 0.3	100 ± 2	153 ± 3
C22-3	22	1150	20.6 ± 0.6	10.0 ± 0.6	87 ± 3	125 ± 3
M22-1	22	1050	16.5 ± 0.6	8.5 ± 0.6	107 ± 2	170 ± 4
M22-2	22	1100	18.7 ± 0.5	9.2 ± 0.4	103 ± 4	153 ± 3
M22-3	22	1150	22.2 ± 0.1	10.4 ± 0.8	92 ± 3	114 ± 2
F22-1	22	1050	21.4 ± 0.5	9.7 ± 0.6	108 ± 4	119 ± 4
F22-2	22	1100	24.6 ± 0.6	10.8 ± 0.5	109 ± 4	95 ± 3
F22-3	22	1150	30.6 ± 0.9	13.4 ± 0.4	92 ± 3	65 ± 4
C17-1	17	1050	13.3 ± 0.4	7.1 ± 0.4	100 ± 4	181 ± 3
C17-2	17	1100	15.1 ± 0.6	7.9 ± 0.3	99 ± 3	157 ± 4
C17-3	17	1150	18.5 ± 0.9	8.9 ± 0.5	85 ± 3	133 ± 4
F40-1	40	1050	25.9 ± 0.7	12.0 ± 0.8	109 ± 3	121 ± 3
F40-2	40	1100	28.8 ± 0.8	12.9 ± 0.6	105 ± 4	105 ± 4
F40-3	40	1150	36.6 ± 1.3	15.8 ± 0.8	92 ± 3	69 ± 3

σ: mechanical strength. E: Young's modulus. $\alpha_{100–650}$: mean linear thermal expansion coefficient in the 100–650 °C range. $\Delta\alpha$: hysteresis of the coefficient of thermal expansion at 573 °C.

the lowest firing temperature, to a reduction in residual quartz content and an increase in glassy phase, which may improve the mechanical properties. The harmful effect of residual quartz in the fired pieces can be readily explained by the cracks around the quartz particles (crack concentration increasing with residual quartz content), which, acting either alone or in combination with large pores, constitute fracture-initiating flaws that contribute to body failure.[13–18] In addition, lower initial quartz particle size may also lead to smaller crack size, should cracking occur, enhancing mechanical strength. Furthermore, these cracks also reduce the Young modulus, as has already been verified in materials with much lower porosity and abundant glassy phase (porcelain, sanitary ware).[36,37]

In order to analyse the effect of microcracking and total porosity, ε, on Young's modulus, it was assumed that the elastic modulus of the porous body without microcracks, E', is directly proportional to the solid area, also known as the Minimum Solid Area (MSA).[38] These models predict, for a broad range of porosity, a familiar exponential relationship of the form:

$$E' = E'_0 \exp(-b'\varepsilon) \quad (4)$$

where b' depends on the type of porosity and E'_0 is the E' value at $\varepsilon = 0$.

If it is assumed that the quartz particles detached from the matrix, Q_d, also reduce the MSA, the resulting effect may, in principle, be assumed to resemble that of ε on the Young modulus, if the quantity of detached quartz is expressed as a volume fraction, ε_c, representing microcrack density. For porous pieces with detached quartz, by analogy with Eq. (4), these premises then yield:

$$E = E_0 \exp(-b(\varepsilon + \varepsilon_c)) \quad (5)$$

By assuming that ε_c is proportional to $\Delta\alpha$:

$$E = E_0 \exp(-b(\varepsilon + k\,\Delta\alpha)) \quad (6)$$

If an effective porosity, ε_{eff}, is defined for these materials as:

$$\varepsilon_{eff} = \varepsilon + \varepsilon_c = \varepsilon + k\,\Delta\alpha \quad (7)$$

Eqs. (4)–(6) become:

$$E = E_0 \exp(-b\varepsilon_{eff}) \quad (8)$$

Eq. (6) agrees well with the experimental values of E, ε, and $\Delta\alpha$. The experimental E data are plotted versus calculated effective porosity ($\varepsilon_{eff} = \varepsilon + \varepsilon_c$) in Fig. 18. All results fit well an exponential relation (variance $s^2 = 3$), according to the proposed model.

The calculated ε_c values are plotted against firing temperature of the pieces in Fig. 19. The results fit quite well three smooth curves (almost straight lines) of negative slope, one for each test quartz particle size. However, the curves corresponding to the pieces obtained with quartz C and M are very similar. The pronounced similarity in the behaviour of the C and M series of pieces suggests that, in both series, the quantity of quartz particles larger than critical size, a_c, is very similar. It was verified by

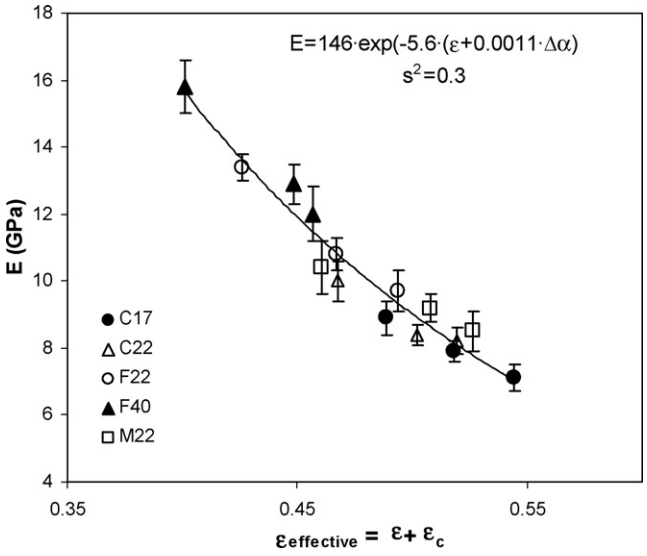

Fig. 18. Experimental E values versus effective porosity.

SEM that the quartz particles smaller than 10–15 μm remained joined to the matrix. Thus, $a_c \approx 10$–15 μm.

Comparison of the particle size distribution of the quartzes used (Table 1) shows that the percentage of particles larger than 15 μm of quartz C (≈75%) and M (≈65%) is very similar, and much larger than that of quartz F (≈25%).

The effect of firing temperature on ε_c may be due to two factors. The first is the decrease in residual quartz content with firing temperature (Fig. 5): according to the literature,[39] this raises critical size, a_c, thus reducing the quantity of quartz detached from the matrix. The second factor is the increased degree of vitrification with firing temperature, which makes it more difficult for quartz grains to detach from the matrix, owing to the larger contact area between both phases.

In order to attempt to determine the dependence of mechanical strength, σ, on characteristics ε and ε_c, Eq. (6), proposed

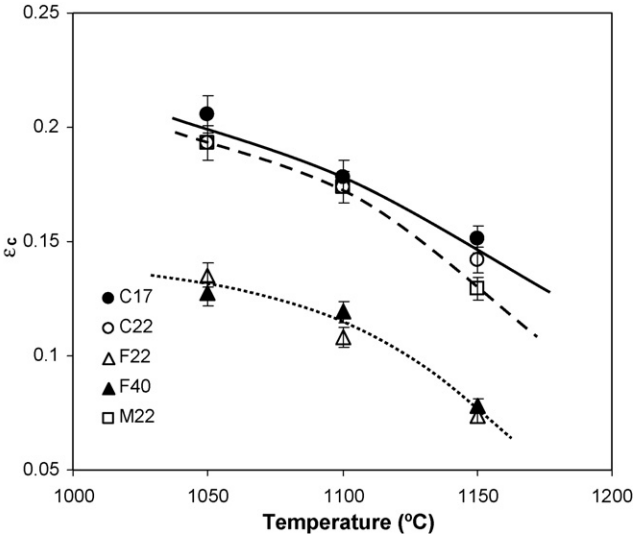

Fig. 19. Microcrack density (as detached quartz volume fraction) versus firing temperature.

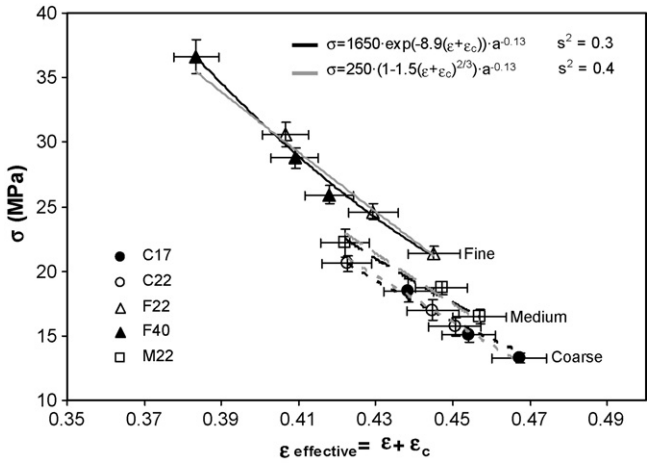

Fig. 20. Mechanical strength as a function of effective porosity.

for E, was first tested, substituting σ and σ_0 for E and E_0. The experimental σ data are plotted versus effective porosity ($\varepsilon + \varepsilon_c$) in Fig. 20. The data fit well three curves of an exponential type, one for each type of quartz. These outcomes confirm the relationship between quartz particle size and fracture-initiating crack size. In view of this, it was attempted to fit the results of Fig. 20 to an equation of the type:

$$\sigma = \sigma_0 \exp(-b(\varepsilon + \varepsilon_c))a^{-n} \quad (9)$$

where 'a' is a representative size of the particle size distribution (PSD) of the quartzes used and n is a constant.

The most frequent quartz particle diameter, the mean quartz particle diameter, and the diameter below which 90% of the quartz particles were found were tested in Eq. (9) as values of 'a'. The best fit was obtained with the last value (variance $s^2 = 0.4$) since, for these materials, as was to be expected, the coarsest particle size, in combination with the largest pores, determines the fracture-initiating crack size.

It has thus been demonstrated in this study that the substitution of an effective porosity, ε_{eff}, for E and σ of total porosity, ε, in the classic models, which takes into account the effect on MSA of total porosity, ε, and microcrack density, ε_c, allows the mechanical properties of these complex materials to be related by simple equations to two microstructural characteristics, ε and ε_c, for the case of E, and to three microstructural characteristics, ε, ε_c, and a, for the case of σ.

The definition and introduction into the classical models of ε_c, which has a simple physical meaning and may be readily estimated, allows the effect of the operating variables on mechanical properties to be reasonably explained.

4. Conclusions

Suspensions were prepared with three mixtures of clay, calcite, and quartz raw materials typically used to manufacture white-firing earthenware tiles, modifying quartz particle size. The rheological behaviour of the suspensions was similar and was typical of highly concentrated, well-deflocculated clay suspensions, only a slight increase in suspension viscosity with a decrease in the quartz particle size being observed. The granules obtained by spray drying these suspensions exhibited similar size and morphological characteristics.

The study shows that when compacts are formed with spray-dried powders at the same pressing pressure, compactness and mechanical strength increase with quartz particle size because this improves particle packing density. In tiles formed with the same compactness (modifying pressing pressure), mechanical strength increased with smaller quartz particle size, as was to be expected. It was further verified that the larger the composition coarse quartz particle fraction (quartz particle size), the larger were the pores in the resulting compacts, independently of the pressing conditions used.

Gehlenite/melilite, anorthite/plagioclase, and wollastonite form during firing: the arising quantity varies with firing temperature but is independent of initial quartz particle size. The residual quartz content in the fired pieces decreases when firing temperature rises and initial quartz particle size decreases. The test pieces fired at 1150 °C displayed more extensive vitrification with increased liquid-phase content. The liquid-phase suppresses small pores, increases the average pore diameter and facilitates quartz dissolution, rounding quartz particle edges and reducing the number of small pores. However, firing shrinkage remains low, and apparent and true porosity hardly changes with firing temperature. All test compacts clearly evidenced microcracking around and inside large quartz particles (above 15 μm). These cracks, acting by themselves or in combination with large pores, constitute fracture-initiating flaws that contribute to body failure.

Microcracking can be correlated with the hysteresis of the coefficient of thermal expansion during heating and cooling. It was observed that, during heating of the fired test piece in a dilatometer, only a fraction of the quartz present in the compact, Q, namely the quartz joined to the matrix, Q_j, contributed to overall expansion, since microcracks separated many quartz particles from the matrix (detached quartz, Q_d), accommodating particle expansion. At dilatometer peak test temperature (900 °C), the quartz particles rebonded to the matrix. In accordance with this observation, the magnitude of the hysteresis (measured as $\Delta\alpha$) must be directly related to microcrack concentration or to the quartz content detached from the matrix, Q_d.

The detached quartz content, Q_d, depends on initial quartz particle size and firing temperature. It was verified that α increases linearly with joined quartz content ($Q_j = Q - Q_d$), and that this relationship is independent of the operating variables (pressing pressure, firing temperature, and quartz particle size) used.

The detached quartz particles, Q_d, have a similar effect to that of porosity on Young's modulus. Indeed, it was verified that if that characteristic is expressed as a volume fraction, ε_c (microcrack density), an effective porosity, ε_{eff}, the sum of total porosity and microcrack density ($\varepsilon_{eff} = \varepsilon + \varepsilon_c$), can be calculated, on which mechanical strength and the modulus of elasticity of the pieces depend, using the classical models of E and σ.

The introduction of ε_c, which has a simple physical meaning and can be readily estimated, into the MSA models enables the effect of the studied operating variables (pressure, temperature,

and quartz particle size) on mechanical properties to be reasonably explained.

The results obtained confirm that the green and fired properties of white-firing earthenware tiles may be considerably enhanced, while holding low shrinkage and high porosity, compatible with low moisture expansion, by reducing quartz particle size and appropriately adjusting the pressing pressure and peak firing temperature. This should enable thin and/or large-sized wall tiles to be manufactured, without (immediate or delayed) curvatures, and with a higher breaking load than that required by the standards.

References

1. Escardino, A., Single-fired ceramic wall tile manufacture. In *Proceedings of the II World Congress on Ceramic Tile Quality, QUALICER. Cámara Oficial de Comercio, Industria y Navegación*, 1992, pp. 117–147.
2. Traoré, K., Kabré, T. S. and Blanchart, P., Gehlenite and anorthite crystallisation from kaolinite and calcite mix. *Ceram. Int.*, 2003, **29**, 377–383.
3. Moreno, A., Ceramic tiles: above and beyond traditional applications. *J. Eur. Ceram. Soc.*, 2007, **27**, 1607–1613.
4. Traoré, K., Ouédraogo, G. V., Blanchart, P., Jernot, J. P. and Gormina, M., Influence of calcite on the microstructure and mechanical properties of pottery ceramics obtained from a kaolinite-rich clay from Burkina Faso. *J. Am. Ceram. Soc.*, 2007, **27**, 1677–1681.
5. Pontikes, Y., Nikolopoulos, P. and Angelopoulos, G. N., Thermal behaviour of clay mixtures with bauxite residue for the production of heavy-clay ceramics. *J. Eur. Ceram. Soc.*, 2007, **27**, 1645–1649.
6. Hajjaji, M. and Kacim, S., Clay–calcite mixes: sintering and phase formation. *Br. Ceram. Trans.*, 2004, **103**, 29–32.
7. Amorós, J. L., Escardino, A., Sánchez, E. and Zaera, F., Dimensional stability in single-fired porous tile. In *Proceedings of the II World Congress on Ceramic Tile Quality, QUALICER. Cámara Oficial de Comercio, Industria y Navegación*, 1992, pp. 347–376.
8. Savage, S. D., Wilson, M. A., Carter, M. A., Hoff, W. D., Hall, C. and Mckay, B., Moisture expansion and mass gain in fired clay ceramics: a two-stage (time) (1/4) process. *J. Appl. Phys. D*, 2008, **41**, 55402.
9. Cole, W. F., On the prediction of long-term natural moisture expansion of fired clay bricks. *J. Aust. Ceram. Soc.*, 1988, **24**, 81–88.
10. Plesingerova, B., Klapac, M. and Kovalcikova, M., Moisture expansion of porous biscuit bodies—reason of glaze cracking. *Ceram. Silik.*, 2002, **46**, 159–165.
11. Sandoval, F., Ibáñez, A., Beltrán, V., González Peña, J. M. and Amorós, J. L., Dolomite marl for fast fired earthenware. *Interceramics*, 1990, **39**(4–5), 38–40.
12. Ibañez, A., Pena, P., Sandoval, F. and González Peña, J., Modification of the inert component in wall tile bodies. *Am. Ceram. Bull.*, 1992, **71**, 1161–1168.
13. Stathis, G., Ekonomakou, A., Stournaras, C. J. and Ftikos, C., Effect of firing conditions, filler grain size and quartz content on bending strength and physical properties of sanitaryware porcelain. *J. Eur. Ceram. Soc.*, 2004, **24**, 2357–2366.
14. Bragança, S. R., Bergmann, C. P. and Hübner, H., Effect of quartz particle size on the strength of triaxial porcelain. *J. Eur. Ceram. Soc.*, 2006, **26**, 3761–3768.
15. Hamano, K., Wu, Y. H., Nakagawa, Z. and Haswgawa, M., Effect of coarse quartz grain on mechanical strength of porcelain body. *J. Ceram. Soc. Jpn. Int. Ed.*, 1991, **99**, 1070–1073.
16. Hamano, K., Wu, Y. H., Nakagawa, Z. and Haswgawa, M., Effect of grain size of quartz on mechanical strength of porcelain bodies. *J. Ceram. Soc. Jpn. Int. Ed.*, 1991, **99**, 149–153.
17. Warshaw, S. I. and Seider, R., Comparison of strength of triaxial porcelains containing alumina and silica. *J. Am. Ceram. Soc.*, 1967, **10**, 337–343.
18. Carty, W. M. and Pinto, B. M., Effect of filler size on the strength of porcelain bodies. *Ceram. Eng. Sci. Proc.*, 2002, **23**, 95–105.
19. Amorós, J. L., Belda, A., Orts, M. J. and Escardino, A., Expansión térmica de piezas de pavimento cerámico gresificado. Influencia de las variables de prensado y de la temperatura de cocción. *Bol. Soc. Esp. Ceram. Vidr.*, 1992, **31**, 109–114.
20. Amorós, J. L., García, J., Orts, M. J., Mestre, S. and Bachero, L., Effect of quartz particle size on the thermal expansion of porous whiteware bodies. In *Proceedings of the VI World Congress on Ceramic Tile Quality, QUALICER. Cámara Oficial de Comercio, Industria y Navegación*, 2000, Pos 35–37.
21. Cleveland, J. J. and Bradt, R. C., Grain size/microcracking relations for pseudobrookite oxides. *J. Am. Ceram. Soc.*, 1978, **61**, 478–481.
22. Manning, W. R., Hunter, O., Calderwood, F. W. and Stacy, D. W., Thermal expansion of Nb_2O_5. *J. Am. Ceram. Soc.*, 1972, **55**, 342–347.
23. Kuszyk, J. A. and Bradt, R. C., Influence of grain size on effects of thermal expansion anisotropy in $MgTi_2O_5$. *J. Am. Ceram. Soc.*, 1973, **56**, 420–423.
24. Hasselman, D. P. H., Donaldson, K. Y., Anderson, E. M. and Johnson, T. A., Effect of thermal history on the thermal diffusivity and thermal expansion of an alumina–aluminum titanate composite. *J. Am. Ceram. Soc.*, 1993, **76**, 2180–2184.
25. Amorós, J. L., Sanz, V., Gozalbo, A. and Beltrán, V., Viscosity of concentrated clay suspensions. Effect of solids volume fraction, shear stress and deflocculant content. *Br. Ceram. Trans.*, 2002, **101**, 185–193.
26. Amorós, J. L., Cantavella, V., Jarque, J. C. and Felíu, C., Fracture properties of spray-dried powder compacts. Effect of granule size. *J. Eur. Ceram. Soc.*, 2008, **28**, 2823–2834.
27. Amorós, J. L., Orts, M. J., García-Ten, J., Gozalbo, A. and Sánchez, E., Effect of green porous texture on porcelain tile properties. *J. Eur. Ceram. Soc.*, 2007, **27**, 2295–2301.
28. Amorós, J. L., Cantavella, V., Jarque, J. C. and Felíu, C., Green strength testing of pressed compacts: an analysis of the different methods. *J. Eur. Ceram. Soc.*, 2008, **28**, 701–710.
29. Jarque Fonfría, J. C., Estudio del comportamiento mecánico de soportes cerámicos crudos: mejora de sus propiedades mecánicas. PhD Thesis, Universitat Jaume I, Castellón, Spain, 2001.
30. Amorós, J. L., Felíu, C., Ginés, F. and Agramunt, J. V., Mechanical strength and microstructure of green ceramic bodies. *Ceram. Acta*, 1996, **8**(6), 5–19.
31. Lee, V.-G. and Yeh, T.-H., Sintering effects on the development of mechanical properties of fired clay ceramics. *Mater. Sci. Eng. A*, 2008, **485**, 2–13.
32. Hajjaji, M. and Khalfaoui, A., Oil shale amended raw clay: firing transformations and ceramic properties. *Constr. Build. Mater.*, 2009, **23**, 959–966.
33. Kara, A., Özer, F., Kayaci, K. and Özer, P., Development of a multipurpose tile body: phase and microstructural development. *J. Eur. Ceram. Soc.*, 2006, **26**, 3769–3782.
34. Isik, G. and Messer, P. F., Effect of compaction pressure on the coarsening of open pores in fired compacts. *Proc. Br. Ceram. Soc.*, 1978, **31**, 39–50.
35. Orts, M. J., Escardino, A., Amorós, J. L. and Negre, F., Microstructural changes during the firing of stoneware floor tiles. *Appl. Clay Sci.*, 1993, **8**, 193–205.
36. Kachanov, M., On the effective moduli of solids with cavities and cracks. *Int. J. Fract.*, 1993, **59**, R17–R21.
37. Lachman, I. M. and Everhart, J. O., Development of safe cooling schedules for structural clay products. *J. Am. Ceram. Soc.*, 1956, **39**, 30–38.
38. Scheffler, M. and Colombo, P., *Cellular Ceramics—Structure, Manufacturing and Applications*. Wiley VCH, Germany, 2005, pp. 291–310.
39. Liu, D. M. and Winn, E. J., Microstresses in particulate-reinforced brittle composites. *J. Mater. Sci.*, 2001, **36**, 3487–3495.